


Article

Three-Dimensional Point Cloud Denoising for Tunnel Data by Combining Intensity and Geometry Information

Yan Bao ¹, Yucheng Wen ¹, Chao Tang ², Zhe Sun ^{1,*}, Xiaolin Meng ³ , Dongliang Zhang ¹ and Li Wang ¹

¹ The Key Laboratory of Urban Security and Disaster Engineering of China Ministry of Education, Beijing University of Technology, Beijing 100124, China; baoy@bjut.edu.cn (Y.B.); wenyucheng@emails.bjut.edu.cn (Y.W.); zhangdongliang@emails.bjut.edu.cn (D.Z.); 202364155@emails.bjut.edu.cn (L.W.)

² Beijing Urban Construction Exploration & Surveying Design Research Institute Co., Ltd., Beijing 100101, China; tangchao@cki.com.cn

³ Faculty of Architecture, Civil and Transportation Engineering, Beijing University of Technology, Beijing 100124, China; mengxl@bjut.edu.cn

* Correspondence: zhesun@bjut.edu.cn

Abstract: At present, three-dimensional laser scanners are used to scan subway shield tunnels and generate point cloud data as the basis for extracting a variety of information about tunnel defects. However, there are obstacles in the tunnel such as pipelines, tracks, and signaling systems that cause noise in the point cloud. Usually, the data of the tunnel point cloud are huge, and the efficiency of artificial denoising is low. Faced with this problem, based on the respective characteristics of the geometric shape and reflection intensity of the tunnel point cloud and their correlation, this paper proposes a tunnel point cloud denoising method. The method includes the following three parts: reflection intensity threshold denoising, joint shape and reflection intensity denoising, and shape denoising. Through the experiment on the single-ring segment point cloud of a shield tunnel, the method proposed in this paper takes 2 min to remove 99.77% of the noise in the point cloud. Compared with manual denoising, the method proposed in this paper takes two fifteenths of the time to achieve the same denoising effect. The method proposed in this paper meets the requirements of a tunnel point cloud data survey. Thus, it provides support for the efficient, accurate, and automatic daily maintenance and surveys of tunnels.

Keywords: shield tunnel; point cloud data; point cloud denoising; point cloud segmentation



Citation: Bao, Y.; Wen, Y.; Tang, C.; Sun, Z.; Meng, X.; Zhang, D.; Wang, L. Three-Dimensional Point Cloud Denoising for Tunnel Data by Combining Intensity and Geometry Information. *Sustainability* **2024**, *16*, 2077. <https://doi.org/10.3390/su16052077>

Academic Editor: Antonio Miguel Martínez-Graña

Received: 31 December 2023

Revised: 25 February 2024

Accepted: 27 February 2024

Published: 1 March 2024



Copyright: © 2024 by the authors. Licensee MDPI, Basel, Switzerland. This article is an open access article distributed under the terms and conditions of the Creative Commons Attribution (CC BY) license (<https://creativecommons.org/licenses/by/4.0/>).

1. Introduction

In recent years, efforts have been made to address the traffic congestion caused by urbanization. Major cities in China are accelerating the planning and construction of fast and high-capacity transportation modes such as subways and light rail. By the end of 2022, a total of 308 urban rail transit operation lines will be opened in 55 cities in mainland China, with a total length of 10,287.45 km [1]. Of these, subway operating lines account for 77.84%, with a total length of 8008.17 km. Other standard urban rail transit operating lines account for 22.16%, with a total length of 2279.28 km. In 2022, the length of newly added operating routes was 1080.63 km, and the cumulative passenger volume for the year reached 19.302 billion people. The total length of the construction plan currently being implemented is 6675.57 km. By the end of the 14th Five Year Plan period, the scale of urban rail transit operation lines will be close to 13,000 km, with over 60 operating cities. The operation scale of urban rail transit continues to expand, and its role as a backbone in public transportation is becoming more apparent. As the role of subway and rail transit in Chinese cities has become increasingly important, its safety has become extremely important. The subway project has huge investment, complex construction, and a long construction period and is considered a century-old project. Therefore, during construction, completion, and

operation and maintenance, the quality requirements are very strict. With the increase in the number of subways, the workload of subway surveys is enormous, and the time windows for subway surveys during operation are relatively short. The traditional survey methods include using the total station to detect ellipticity and using a ruler to detect platform dislocation. The total station is an improved version of the theodolite with auto-leveling and electronic rangefinder. However, these methods do not have automation functions and need manual surveys. In the process of measurement, the instrument needs to be moved and leveled frequently, which leads to low efficiency. Therefore, it is necessary to conduct research on the efficient, accurate, and automated daily maintenance and survey of subway tunnels to meet the requirements of subway construction and operation processes.

Currently, mobile 3D laser scanners are commonly used tools for tunnel surveys. These can quickly obtain the surface information of the scanning area and generate point cloud data. Point cloud data are a collection of discrete points that represent the surface information of objects in three-dimensional space. They include three-dimensional coordinates and laser reflection intensity for each point. In point cloud data, the X-axis of the coordinate system represents the horizontal direction of the tunnel cross-section, the Z-axis represents the vertical direction, and the Y-axis represents the direction in which the car moves forward (i.e., the mileage direction). The point cloud reflection intensity refers to the reflected energy intensity of each point recorded by a 3D laser scanner during the scanning process. When the laser beam is irradiated on the target surface, some of the light is reflected back by the target object. The laser scanner will measure and record the energy intensity of this reflected light, and the reflection intensity of different objects varies. The reflection intensity value is also affected by factors such as distance and equipment parameters. In the tunnel, the influence of atmospheric conditions on reflection intensity is temporarily not considered.

The information of daily maintenance and surveys of subway can be quickly extracted from point cloud data, which can effectively carry out subway surveys every day. To meet the accuracy requirements of various surveys, point cloud data need to be denoised. In most daily maintenance and inspection projects, such as the ovality and step of tunnels, only point cloud information of pipe segments is required. However, the tunnel point cloud data obtained via scanning include point cloud data on segments, pipelines, tracks, supports, and various ancillary equipment. At this time, for survey work, the point cloud information of pipelines, tracks, supports, and various ancillary equipment will be regarded as noise. Noise can have a significant impact on the analysis results, so it is necessary to remove the noise.

In addition to three-dimensional and intensity information, there is also more basic information in point cloud data, such as color information, point cloud density, and normal vectors. Currently, utilizing three-dimensional information for denoising is the most common approach, but usually, further processing is carried out on three-dimensional information. Zhu [2] obtained curvature features from the three-dimensional information of point clouds and then performed denoising on the point clouds. Some authors consider point cloud density. Zhao [3] proposed a point cloud denoising algorithm based on curvature and point cloud density. For points used for surface reconstruction, Zama [4] proposed using a denoising method based on point cloud density. For ring forgings containing noise, Zhang [5] extracted profile lines based on point cloud normal vectors. Liu [6] proposed using point cloud normal vectors and curvatures to smooth out noise in hydraulic torque converters. These denoising methods all process the three-dimensional information of point clouds, requiring a large amount of computation for each point, resulting in a longer processing time.

At present, there are many denoising methods using 3D information, such as filter-based denoising, optimization-based denoising, and deep learning-based denoising. Wei [7] uses the dual normal filtering algorithm to denoise irregular surfaces. Mattei [8], Dai [9], and Zheng [10] all specialize in processing sharp features of point clouds, using MRPCA denoising, position filtering denoising, and guided normal filtering denoising, respectively.

Liang [11] uses an adaptive optimal neighborhood algorithm for denoising scattering point cloud models. Gao [12] transformed the point cloud denoising problem into an optimization problem of the prior regularization of graphic signal smoothness. Sun [13] uses L0 minimization for denoising, but the boundaries cannot be well handled. Some authors use denoising networks for denoising. Li [14] targets unordered noise, while Yan [15] targets noise in the engine model. The above denoising methods can meet the needs in their respective fields, but most methods only use three-dimensional coordinate information for denoising, while other basic information of point clouds is rarely used.

The core method of Irfan [16] and Cao [17] denoises through color information, but Irfan further combines geometric information to construct k-NN graphs for denoising. However, there are some limitations in denoising through color information, and it is difficult to remove the noise of the same color. Choi [18] and Clode [19] denoise by setting a threshold range for the reflection intensity value, but the calculation of the threshold range is still entirely based on the reflection intensity information. Most of these methods only use one piece of information of the point cloud for denoising. This paper also uses reflection intensity to denoise, so it is necessary to study the problems existing in intensity denoising. Although only using the threshold value of reflection intensity can remove some noises, there are still many noises with similar reflection intensity values that cannot be removed.

Faced with this situation, we propose a denoising method for tunnel point clouds, which includes reflection intensity threshold denoising, joint shape and reflection intensity denoising, and shape denoising. Among them, the joint shape and reflection intensity denoising method comprehensively considers the correlation between the tunnel geometry and reflection intensity of the point cloud. This method is also suitable for other situations where the strength value changes uniformly, such as the measurement of a circular shield working shaft. This proposed method aims to provide high-quality point clouds and provide a reliable basis for the subsequent analysis of and application to tunnels.

Before denoising the point cloud data of shield tunnels in this paper, preprocessing is required. The first step in preprocessing is to segment each segment ring from the point cloud data. A segment ring is a complete lining ring composed of multiple segments. This approach can break down a large computational task into multiple small tasks, thereby improving computational efficiency. Next, unfold the point cloud data of each segmented segment, and partition the point cloud data into multiple parts along the unfolding direction. Once the pre-processing of the point cloud data is complete, the denoising process begins. This paper has three steps for point cloud denoising. The first step is the threshold denoising method of reflection intensity. This step involves setting an appropriate reflection intensity threshold range to remove point cloud data with intensity values exceeding that threshold range. The next step is to denoise the shape and reflection intensity jointly. In this method, the intensity value of the unfolded point cloud data is processed by the optimized quartile range method and the Z score method. The last step is the geometric shape denoising method. This step involves setting a distance threshold based on the design radius of the segment and the fitted elliptical curve and removing point cloud data outside the distance threshold. By using the above steps to denoise the point cloud data of shield tunnels, the quality and accuracy of the data can be improved, providing a reliable foundation for subsequent analysis and application.

The organizational structure of this paper is as follows. In the Section 1, the background and research questions are introduced. The Section 2 provides a detailed introduction to the preprocessing and denoising steps of point cloud data. The feasibility of the algorithm was verified through practical engineering examples, which are outlined in the Section 3. The Section 4 verifies the denoising results of the algorithm. The Section 5 provides some conclusions and future plans.

2. Denoising Methods

This section introduces each step of the denoising method in detail. First, before denoising, some processing of point clouds is beneficial to efficient denoising. The first step is to segment each segment ring from the point cloud data. The second step is to unfold the point cloud of the segment. Next, denoise the point cloud. The third step is to process point clouds by the reflection intensity threshold method. The fourth step is to combine the denoising methods of shape and reflection intensity to process the point cloud. The fifth step is the geometric shape denoising method to process the point cloud. The denoising flowchart is shown in Figure 1.

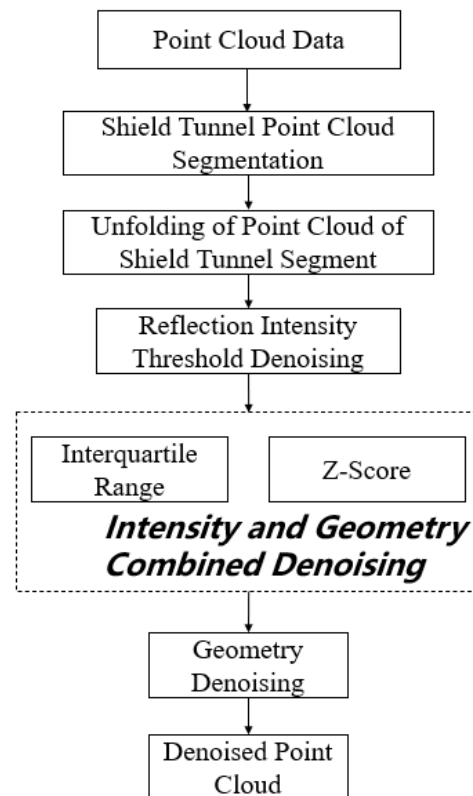


Figure 1. Denoising flowchart.

2.1. Shield Tunnel Point Cloud Segmentation

The complete point cloud data of a shield tunnel usually comprise several hundred gigabytes, which is a large amount of data to process. Therefore, before denoising the point cloud, it is necessary to segment the point cloud data, which helps to reduce the complexity of data, improve processing efficiency, and better manage and utilize large-scale point cloud datasets. By segmenting point clouds, a series of data subsets can be obtained, making further processing, analysis, and application more effective. In shield tunnels, there are assembly gaps between adjacent ring segments. These gaps will cause changes in the scanning distance, leading to changes in the intensity value of point cloud data, as shown in Figure 2. This paper utilizes the variation information of point cloud intensity values to accurately segment the point cloud of pipe segments. In order to avoid the impact of equipment such as pipelines, tracks, and signal boxes in the tunnel on point cloud segmentation, the point cloud data at the top of the tunnel are selected for analysis.

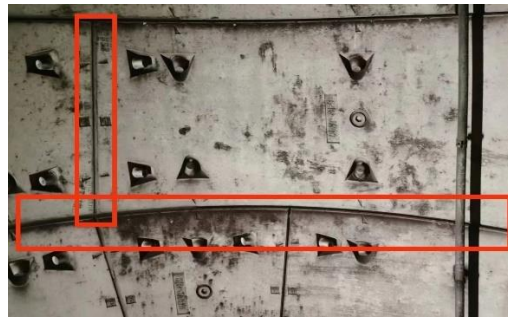


Figure 2. Assembly gap.

However, using point cloud data from the entire top of the tunnel for calculation can result in significant computational complexity. Therefore, some cloud points (6 degrees) are selected from the top of the tunnel to replace the point clouds at the top of the whole tunnel. Point cloud segmentation is calculated by the selected part of the point cloud, as shown in Figure 3a. It can reduce computational complexity and improve work efficiency while ensuring accuracy.

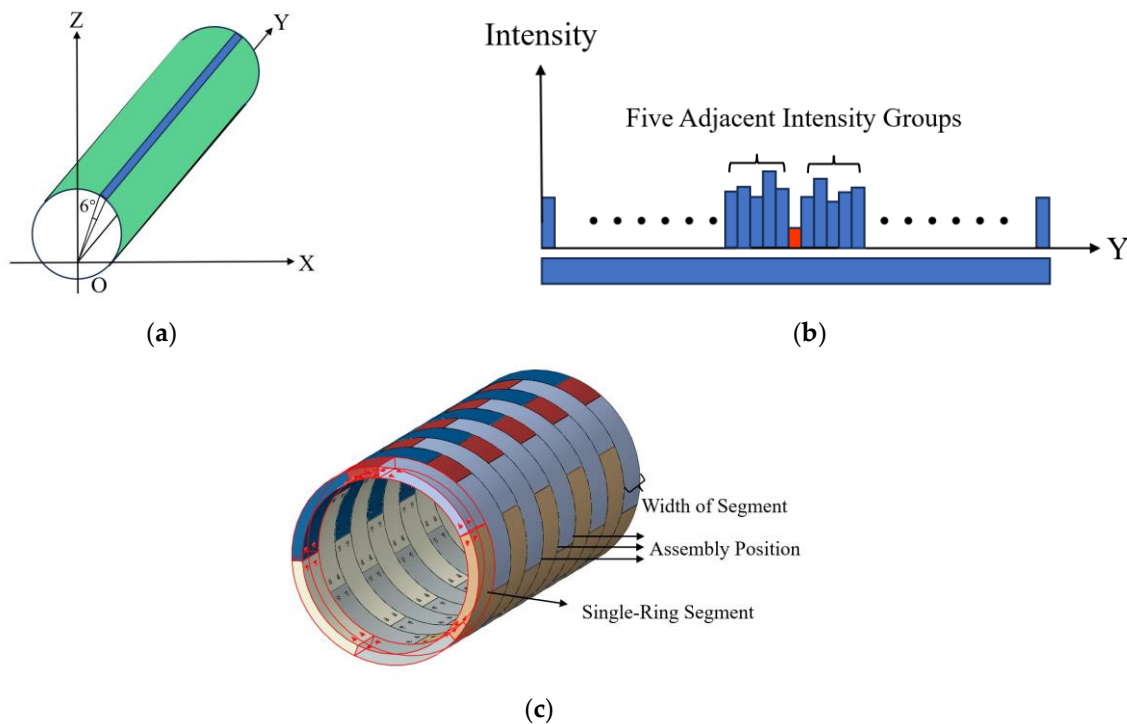


Figure 3. (a) The blue part is the selected point cloud. (b) The Y-average reflection intensity plot (red marks are intensity values that are smaller than adjacent intensity values). (c) Schematic diagram of shield segment assembly (different colors indicate different segments, and six segments form a single-ring segment).

Point cloud data are grouped in groups of 40 mm on the mileage (Y axis), and the average value of the intensity values of all points in each group is calculated as the intensity value of this group of points, as shown in Figure 3b. Calculate the difference between the intensity value of each group and its five groups of adjacent intensity values before and after. By comparing the differences, the intensity value that is much smaller than the adjacent intensity value is calculated. The grouping position of these smaller strength values is the assembling position between each ring segment. To verify the accuracy of the position, the distance between these smaller intensity values is calculated. If the separation distance is

the width of segment, then the positions are accurate. The point cloud is segmented into single-ring segments at the assembly position, as shown in Figure 3c.

2.2. Unfolding of Point Cloud of Shield Tunnel Segment

After dividing the point cloud data, in order to perform denoising processing, it is necessary to unfold the point cloud data. Because the mobile 3D laser scanner travels on the track of the tunnel, the center of the scanner is horizontally located on the axis of the tunnel. However, in the vertical direction, due to the height limitation of the scanner, the center of the scanner is not located on the axis of the tunnel, as shown in Figure 4. Therefore, the Y-axis in the coordinate system of the point cloud data does not coincide with the axis of the tunnel. Before unfolding, it is necessary to process the Z-values of all point clouds so that the Y-axis in the coordinate system of the point cloud data coincides with the axis of the tunnel. In addition, ensure that the coordinate origin is located on the axis of the tunnel.

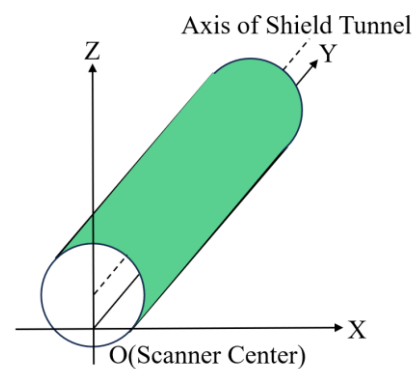


Figure 4. Point cloud coordinate system.

After processing the point cloud coordinates, project the point cloud onto the XOZ plane. The coordinates of any point P in the projected point cloud are (x, z). The radian is used as the unit of point cloud unfolding, which is an angular unit and dimensionless [20]. During the unfolding process, the radian is based on the negative direction of the Z-axis, and counterclockwise rotation is considered positive, namely, $Rad \in [-1.57rad, 4.71rad]$, as shown in Figure 5. In the figure, A is $-\pi/2$, which is approximately -1.57 , and B is $3\pi/2$, which is approximately 4.71 . The formula for calculating radians is shown in Equation (1). During the unfolding process of the tunnel point cloud, other values in the point cloud data remain unchanged. Due to the obstruction of the track, the point cloud of the bottom segment cannot be scanned, so the bottom point cloud is considered noise. Therefore, point clouds within the range of 0.5 rad to 8.5 rad were selected for denoising.

$$\begin{cases} rad = \tan^{-1}\left(\frac{z}{x}\right), & x \in (0, +\infty) \\ rad = \tan^{-1}\left(\frac{z}{x}\right) + \pi, & x \in (-\infty, 0) \end{cases} \quad (1)$$

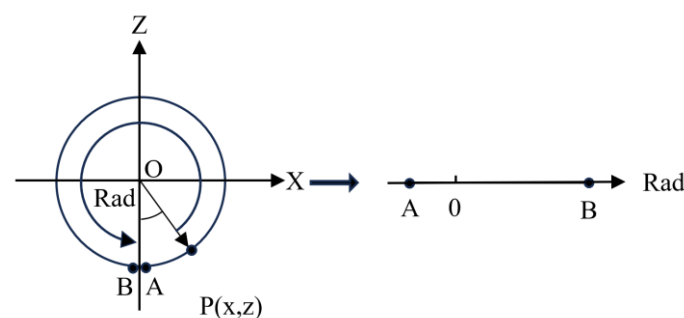


Figure 5. Schematic diagram of point cloud unfolding.

2.3. Reflection Intensity Threshold Denoising

After preprocessing the point cloud data, the point cloud is first denoised using the reflection intensity threshold method. The shield tunnel contains objects such as segments, pipelines, tracks, supports, and other equipment. They all have different materials, so their surface reflectivity and reflection intensity will also vary. By setting a threshold range for reflection intensity, only points within the threshold range are retained. The points that exceed the threshold are taken as noise and removed. When determining the threshold range of the point cloud reflection intensity, it is necessary to consider the distribution of the point cloud intensity and the reflection intensity of the segments and adjust it based on specific application scenarios and data characteristics. The threshold range can be found directly in the point cloud, through the different intensity values of points at different positions in the segment, or the distribution of intensity values in the point cloud is counted, and the threshold range can be selected according to the concentration range of intensity values.

However, relying solely on reflection intensity threshold denoising methods cannot remove all noise points. In the point cloud of a shield tunnel, noise may have reflection intensity values similar to the target point. So, the reflection intensity threshold denoising can only remove noise with obvious differences and cannot remove noise with similar intensity values. Therefore, when applying the threshold denoising method for reflection intensity values, it is necessary to comprehensively consider other denoising methods and data characteristics in order to achieve better denoising results.

2.4. Intensity and Geometry Combined Denoising

The joint denoising of the shape and reflection intensity is also a method of denoising through point cloud intensity values, which combines the geometric shape of point clouds and reflection intensity values. Due to the distance effect, objects of the same material may produce different reflection intensities, while objects of different materials may produce the same reflection intensity. This seriously affects the effectiveness of using the reflection intensity threshold for denoising. To address this issue, this method not only takes into account the variation in strength values of each point itself but also takes into account the geometric shape characteristics of the tunnel point cloud. For the geometric shape characteristics of tunnel point clouds, this paper considers the variation of strength values between each point and its adjacent points. When it is necessary to extract the same material point cloud from a point cloud, a situation may occur where the points are geometrically distant from each other, but the intensity values of the points are the same (the material and distance have a comprehensive impact on the intensity values).

For mobile 3D laser scanners in shield tunneling subway tunnels, the instrument center point during the scanning process is not at the center of the cross-section design circle. Therefore, when the laser head of the scanner rotates once, the distance from the laser to the segment surface at different angles changes uniformly. If the strength value of the same material is only affected by the change in scanning distance, and this change is uniform, the intensity value will also vary uniformly. Therefore, after unfolding the point cloud, the point cloud intensity value of the segment should exhibit a uniformly changing curve. When an abnormal intensity value occurs in a uniform variation of intensity values, the point corresponding to the abnormal intensity value is noise. This abnormal intensity value may be caused by two factors: first, different target materials, which lead to different reflectivities, and second, different distances. Based on this situation, this paper proposes a joint denoising approach of shape and reflection intensity. First, the point cloud is processed according to the method in Section 2.2. After that, the point cloud data are divided into 200 groups of points according to a group of 0.04 rad in radian. Finally, the intensity values of each group of points are processed by IQR and Z-Score.

2.4.1. Interquartile Range

The IQR (interquartile range) is a robust method used to label outliers [21]. The IQR method for detecting outliers was developed by John Tukey, who was a pioneer in exploratory data analysis. Arrange the dataset from small to large, and partition it into four equal parts; the values at the three dividing points are quartiles, namely, Q1 (the lower quartile), Q2 (the median), and Q3 (the upper quartile). The box-whisker plot uses quartiles to plot the shape of data, as shown in Figure 6. The box represents Q1 and Q3, and the lines inside the box represent Q2, which is the median. The interquartile range (hence the name of the outlier detection method) is the distance between Q1 and Q3 (box edges), $Q3 - Q1$. Tukey considered data located outside $Q3 + 1.5 \times IQR$ (Upper $1.5 \times IQR$ whisker) or $Q1 - 1.5 \times IQR$ (Lower $1.5 \times IQR$ whisker) to be outliers. The whisker line extends to the last data point within the boundary.

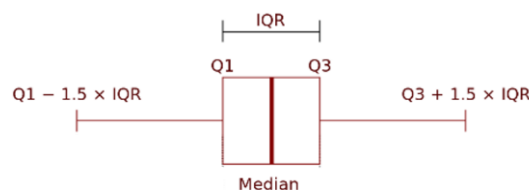


Figure 6. Box-whisker plot.

In order to meet the needs of joint denoising of shape and reflection intensity, the box-whisker plot is improved, as shown in Figure 7. First, set the size range for the box-whisker plot boundary. The next step is to detect the boundary value of the box-whisker plot. Finally, smooth and continuous processing is carried out between adjacent box-whisker plots. The detailed steps are as follows:

1. Calculate the box-whisker plot of each group of points: Calculate the interquartile range of each group of points, and calculate the box-whisker plot of each group of points according to the quartile, so that each group of points has a box-whisker plot.
2. Set the size range of the box-whisker plot boundary: Calculate the difference between $Q3 + 1.5 \times IQR$ and $Q1 - 1.5 \times IQR$ and set the boundary size range. In each group of points, the rotation of the scanner is small, so the laser distance changes little, and thus, the intensity value changes little. Therefore, the segment strength values in each group of points are concentrated near one value. By setting the maximum limit range and the minimum limit range, it can prevent the inclusion of abnormal values and the removal of target values.
3. Boundary value detection: Calculate the distance from the edge point to the nearest boundary, and if it is less than a certain value, take the edge point as the boundary value. This ensures that multiple filters do not delete all values, retaining more valid points and point cloud data accuracy.
4. Check the position of the box-whisker plot: It is necessary to check the position of each box-whisker plot to ensure that each box-whisker plot and its adjacent box-whisker plot meet the requirements of smoothness and continuity. When smoothing is detected, the slope of Q2 between adjacent boxes is calculated, and the slope threshold is set. If the slope exceeds the threshold, it needs to be smoothed. In this paper, the interpolation method is adopted to deal with it, and Q2 of the box-whisker plot exceeding the threshold is set as the interpolation of Q2 of the previous box-whisker plot and the next box-whisker plot. The boundary of the box-whisker plot changes with Q2. The reason why the positions of some adjacent box-whisker plot are quite different is that there are almost no segment points in this group, which are basically noise caused by obstructions.

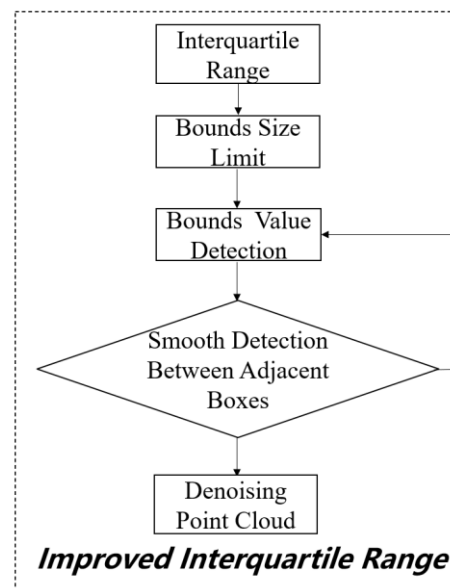


Figure 7. Improved interquartile range.

2.4.2. Z-Score

The Z-score describes a data point in relation to the mean and standard deviation of a set of points [22]. It maps the data to a distribution with a mean of 0 and a standard deviation of 1. The purpose of using Z-scores is to eliminate the influence of the data position and scale, allowing for direct comparison across different datasets. The logic behind the Z-score outlier detection method is that once the data are centered and rescaled, any values that deviate significantly from zero should be considered outliers. The Z-score method relies on the mean and standard deviation of a set of data to measure its central tendency and dispersion. However, since the mean and standard deviation are highly influenced by outliers, they are not robust measures. The presence of outliers causing skewness is one of the main reasons for identifying and removing outliers from a dataset. Another drawback of the Z-score method is its poor performance on small datasets. In fact, if the number of items in the dataset is less than 12, the Z-score method fails to detect outliers. This led to the development of the modified Z-score method, which overcomes these limitations, shown in Equation (2). This method is particularly suitable for skewed data or data with a non-normal distribution and a small number of observations. The MAD (median absolute deviation) is a robust measure of central tendency and dispersion used in the modified Z-score method. One advantage of the modified Z-score method is that it uses the median and MAD instead of the mean and standard deviation. The median and MAD are robust measures that provide a more robust assessment of central tendency and dispersion.

$$M_i = \frac{0.6745(x_i - \tilde{x}_i)}{MAD}, \quad (2)$$

2.5. Geometric Denoising

Geometric shape denoising is a method based on the geometric features of shield tunnel point clouds, which denoises by setting different ranges of circles and ellipses [23]. This method identifies and removes noise by using the distance between the point in the point cloud and the center of the tunnel. This method uses circles and ellipses as distance thresholds. Identify points within the distance threshold as valid points, and identify points outside the distance threshold as noise and remove them. By adjusting the size of circles and ellipses, the range of denoising can be controlled. First, the ellipse is fitted once to determine the center point of the tunnel segment. Afterward, by increasing and decreasing a certain value of the design radius, a circular range is formed, and points outside the

circular range are treated as noise and removed. Next, fit the ellipse again to obtain the center point of the segment and the elliptical equation. By increasing and decreasing the values of the major and minor axes of the ellipse, two ellipses are obtained, forming a circular range. Similarly, treat points outside the torus as noise and remove them.

The advantages of geometric shape denoising methods are that they are simple, intuitive, and easy to implement. However, this method also has some limitations and precautions. The selection of the distance threshold needs to be adjusted according to the characteristics of specific data and application needs. If the threshold selection is too small, the target point may be erroneously removed. If the threshold selection is too large, it may not be possible to effectively remove noise points. Therefore, in this method, geometric shape denoising is used as a supplement to the intensity value denoising method. By comprehensively applying multiple denoising methods to process point clouds, better denoising effects and data quality can be achieved.

3. Experimental Results

In order to verify the practicality of the algorithm, this paper takes a shield tunnel in a certain section as an example to carry out the experiment. The tunnel had a total length of 575 m and was constructed using the shield tunneling method. It had an inner diameter of 5.4 m, an outer diameter of 6 m, and a segment width of 1.5 m. We used a mobile 3D laser scanner to obtain point cloud data of shield tunnel segments. We rendered the point cloud based on its intensity values, as shown in Figure 8a,b. By analyzing the point cloud strength values of shield tunnel segments, we found that the strength values were mainly concentrated within the range of [100, 160], as shown in Figure 8c.

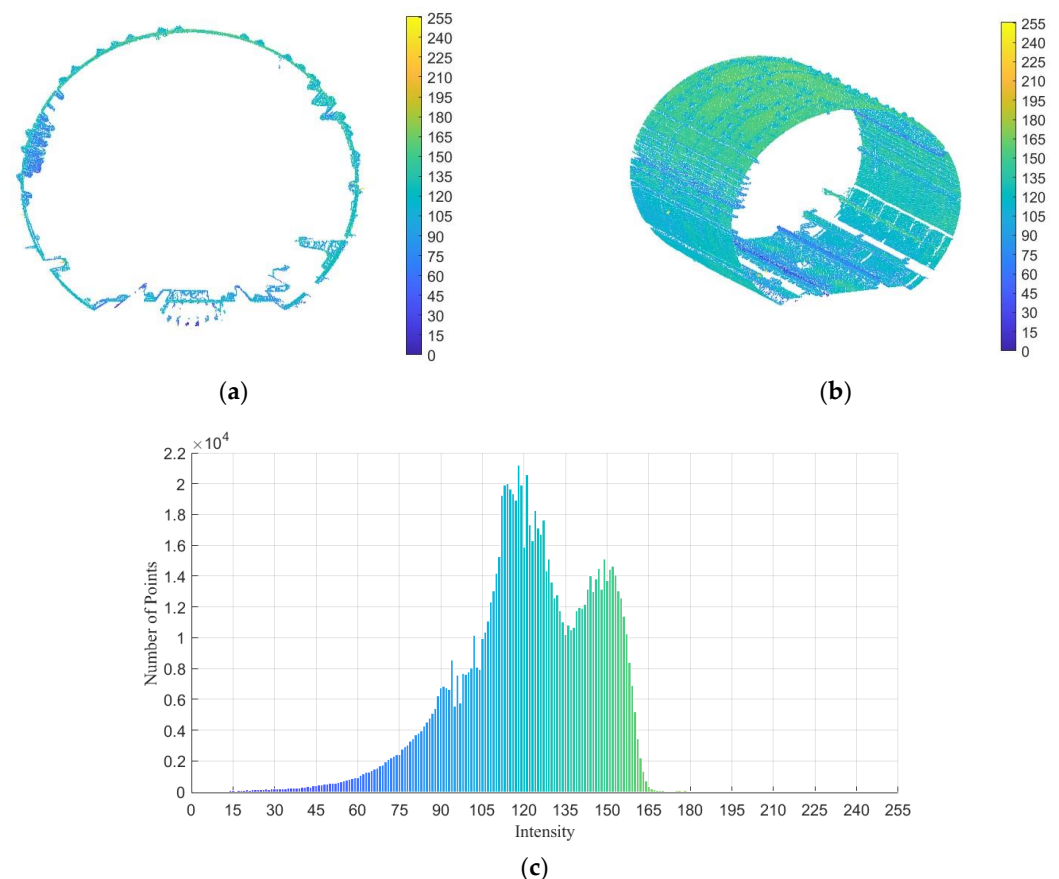


Figure 8. (a) Cross-sectional view of reflection intensity of multi-ring point cloud. (b) Reflection intensity of multi-ring point cloud. (c) Multi-ring point cloud intensity distribution (the color is rendered as intensity value, and the chromatogram is as shown in (a)).

Because the segmentation with complete point cloud data requires a huge amount of data, it will lead to extremely low computational efficiency. Point cloud segmentation helps to reduce the complexity of data and improve the processing efficiency. So, according to the method in Section 2.1, some point cloud data above the top of the tunnel are selected for segmentation, and the selected data are shown in Figure 9.

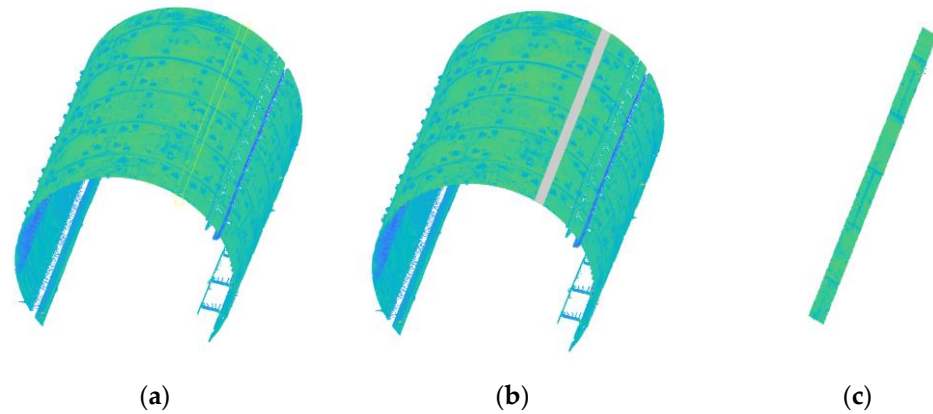


Figure 9. (a) Complete point cloud. (b) Selected point cloud position (gray is the selected part). (c) The selected point cloud (the color is rendered as intensity value, and the chromatogram is as shown in Figure 8a).

We projected the selected point cloud data onto the XOY plane, as shown in Figure 10a, and drew a mileage intensity map of the point cloud, as shown in Figure 10b. The horizontal axes in Figure 10a,b are the same and can be observed correspondingly. Observation shows that with every 1.5 m change in mileage, the point cloud intensity value suddenly decreased. These reduced strength values corresponded to the assembly positions between adjacent ring segments. These assembly gaps can cause changes in the scanning distance, resulting in changes in the intensity value of the point cloud data obtained through scanning.

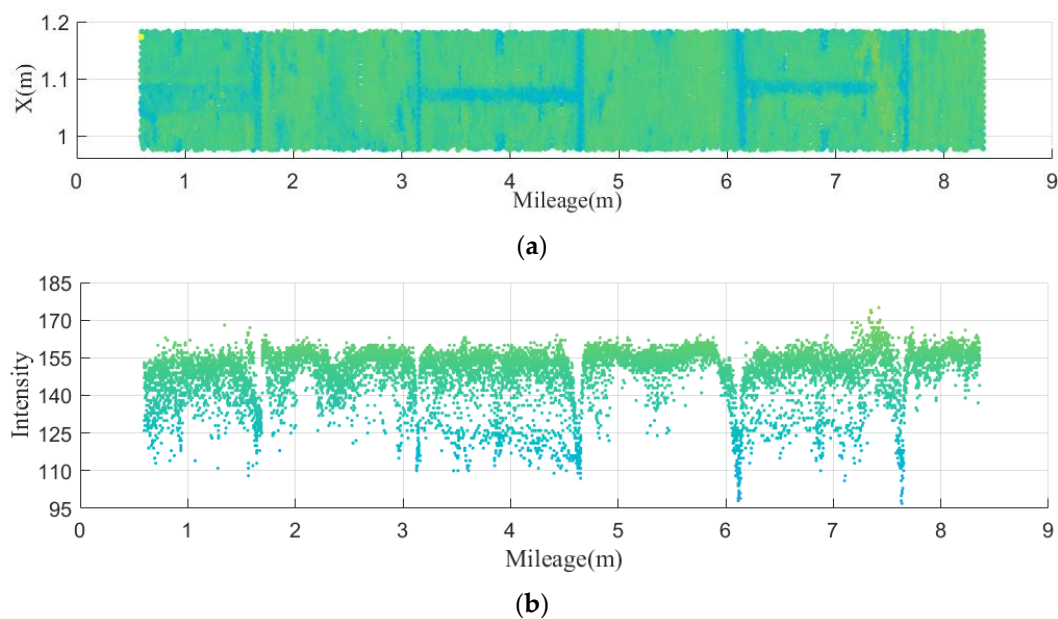


Figure 10. (a) Mileage–X plot of selected point cloud. (b) Mileage–intensity plot of selected point cloud (the color is rendered as intensity value, and the chromatogram is as shown in Figure 8a).

According to Section 2.1, the intensity values were partitioned into 200 groups by mileage, and the average value of each intensity value was calculated. We drew an average

intensity map and highlighted the data with significant differences between the average intensity and the surrounding area in red, as shown in Figure 11. The mileage of the red difference data in Figure 11 is compared with Figure 10, where the red difference data are located at the junction of segments. The red difference data interval was about 1.5 m, which was consistent with the actual width of the shield tunnel segments.

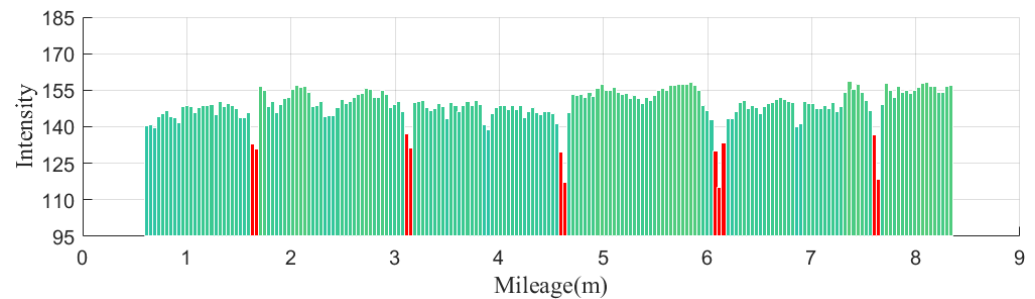


Figure 11. Intensity average plot (red marks are the intensity value that are significantly different from adjacent intensity values).

The shield tunnel point cloud was cut out according to the mileage of the red difference data, as shown in Figure 12a,b. The intensity distribution of a ring point cloud was analyzed, as shown in Figure 12c.

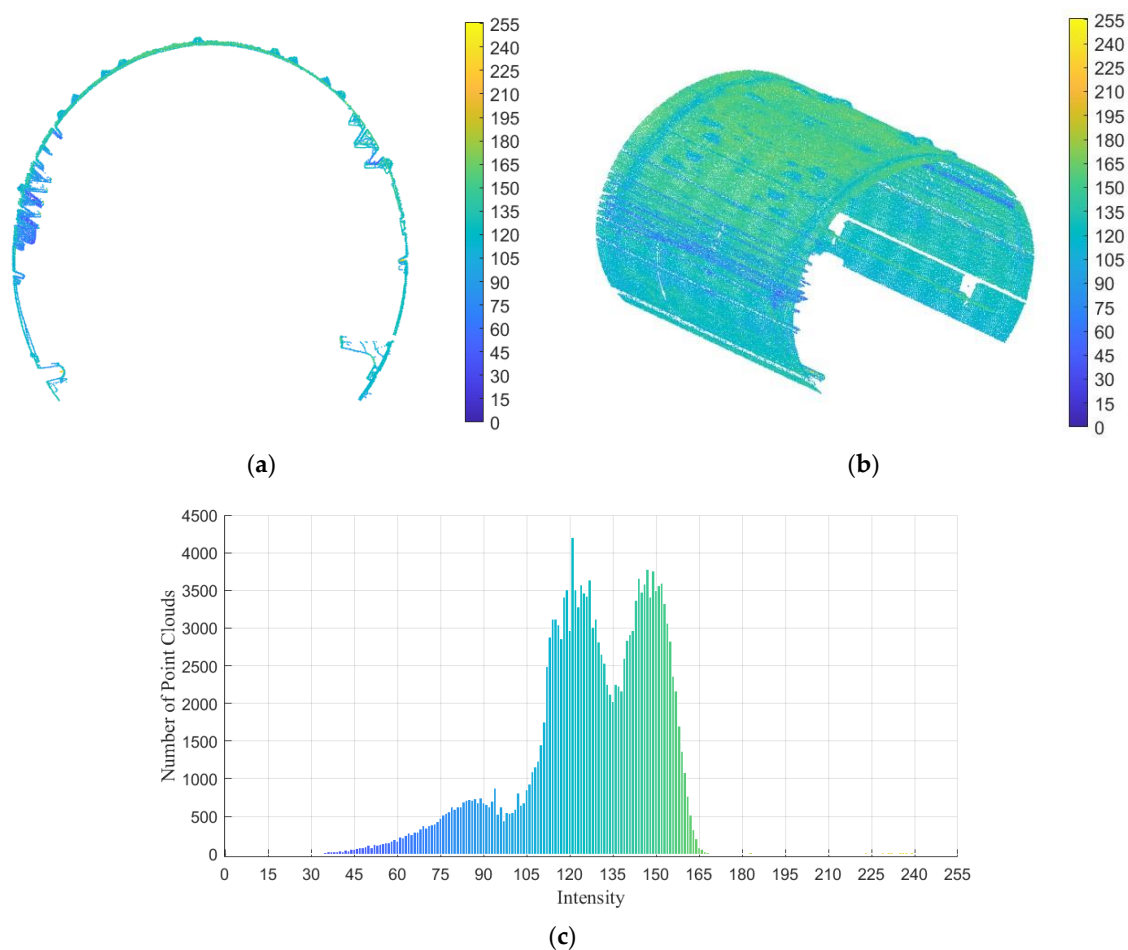


Figure 12. (a) Cross-sectional view of reflection intensity of single-ring point cloud. (b) Reflection intensity of single-ring point cloud. (c) Intensity distribution of single-ring point cloud (the color is rendered as intensity value, and the chromatogram is as shown in Figure 8a).

According to the method given in Section 2.2, we unfolded the point cloud data of the first ring shield tunnel. We rendered the point cloud based on intensity values, as shown in Figure 13. From Figure 13, it can be clearly seen that the strength of the pipe segment gradually changed with the curvature. The change in the intensity value was due to the scanner not being located at the center of the tunnel section, resulting in changes in the distance as the laser reached the surface of the pipe from different angles.

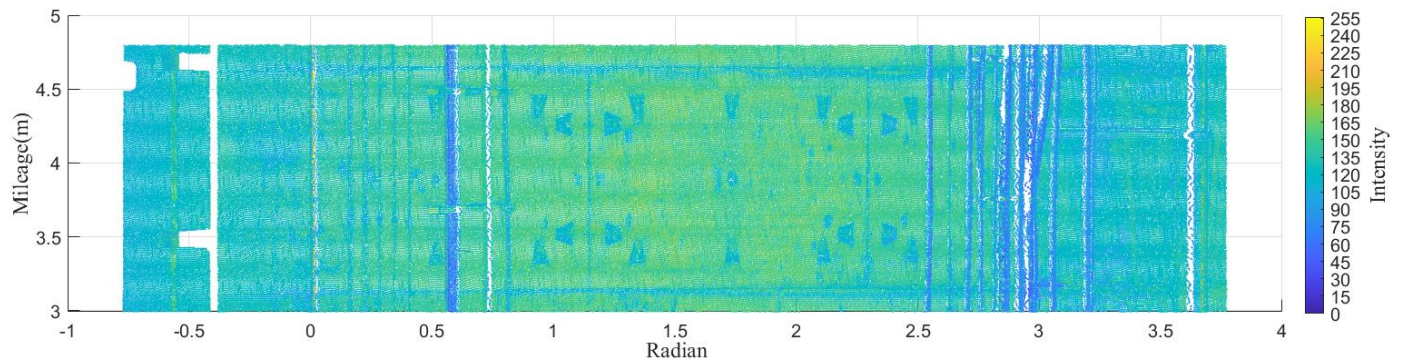


Figure 13. Single-ring point cloud expansion.

After unfolding the point cloud data into a plane, the intensity value of the point cloud could be added as an additional dimension, as shown in Figure 14. Then, we drew a single-loop radian–intensity diagram, as shown in Figure 15. The intensity value of the segment point cloud was only affected by the distance of uniform variation, so the intensity value showed a trend of uniform variation. In Figure 15, the intensity values are a uniformly changing curve, but there are many abrupt abnormal intensity values in the curve. The intensity values of these mutations are the noise to be removed.

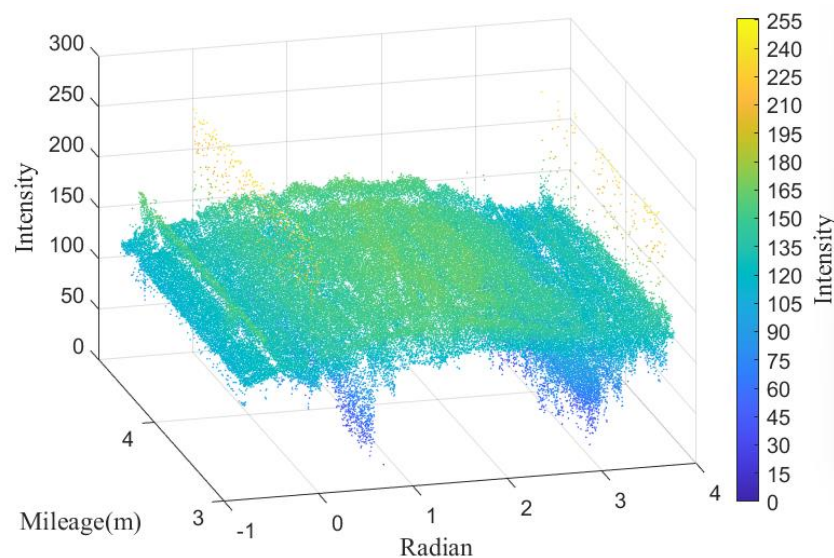


Figure 14. Point cloud unfolding intensity.

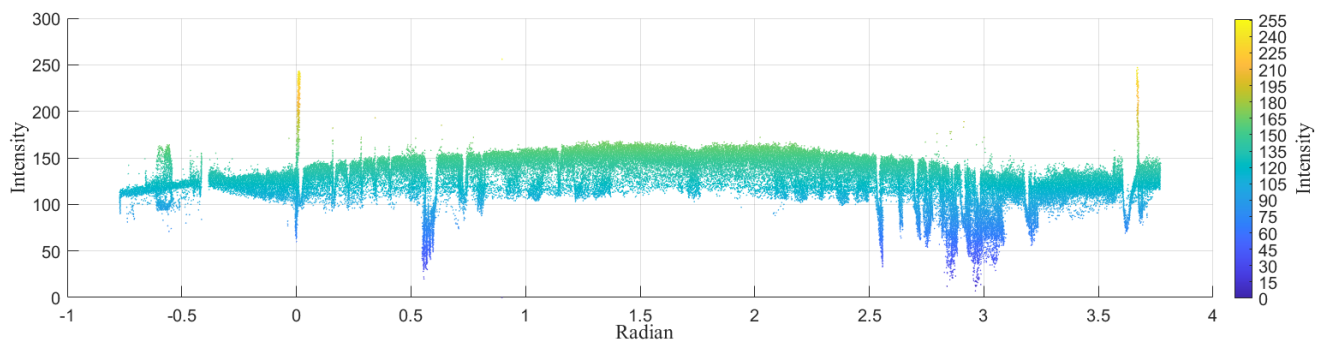


Figure 15. Single-ring radian-intensity plot.

First, according to the method in Section 2.3, noise was removed by the intensity threshold method. As shown in Figures 12c and 13, we set the threshold range of point cloud intensity values to [100, 160] and removed points outside the threshold range.

Next, the intensity values of the single-ring point cloud were partitioned into 200 groups according to radians. Then, according to the method in Section 2.4, denoising was carried out through the combination of shape and reflection intensity. For each segment point cloud intensity value, we denoised using the optimized IQR and Z scores. The denoising method removed the point cloud of intensity values that varied dramatically in a uniformly changing curve. It could remove points that exhibited drastic changes in a uniformly changing intensity curve. The radian-intensity graph after denoising is shown in Figure 16a. Figure 16b shows the radian-intensity plot of the removed tunnel noise points.

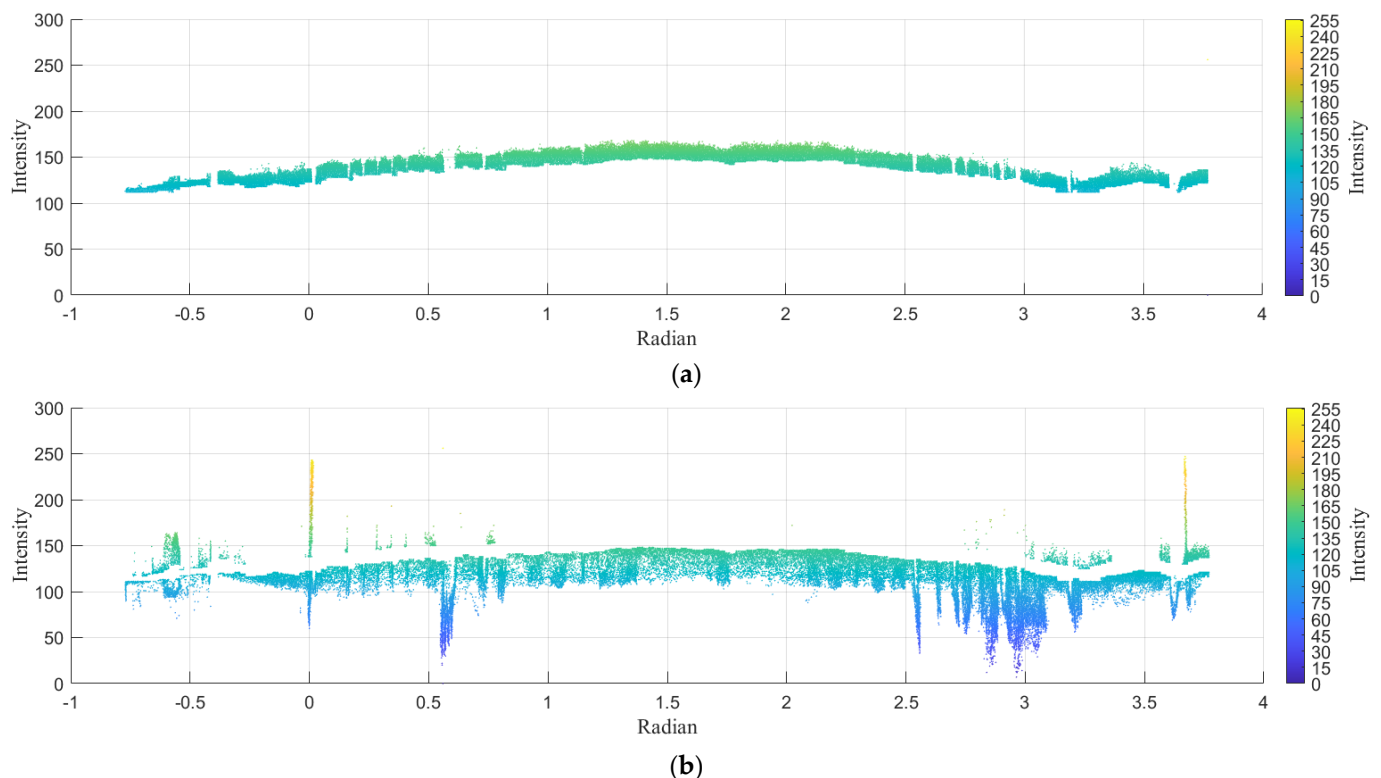


Figure 16. (a) Radian-intensity plot after denoising. (b) Radian-intensity plot of removed tunnel noise points.

We compared the tunnel point cloud cross-sectional images before and after denoising. An image from before denoising is shown in Figure 17a, and an image from after denoising is shown in Figure 17b. From the point cloud cross-sectional view, it can be seen that many

noise points such as pipelines and supports in the tunnel before denoising were mostly removed after denoising.

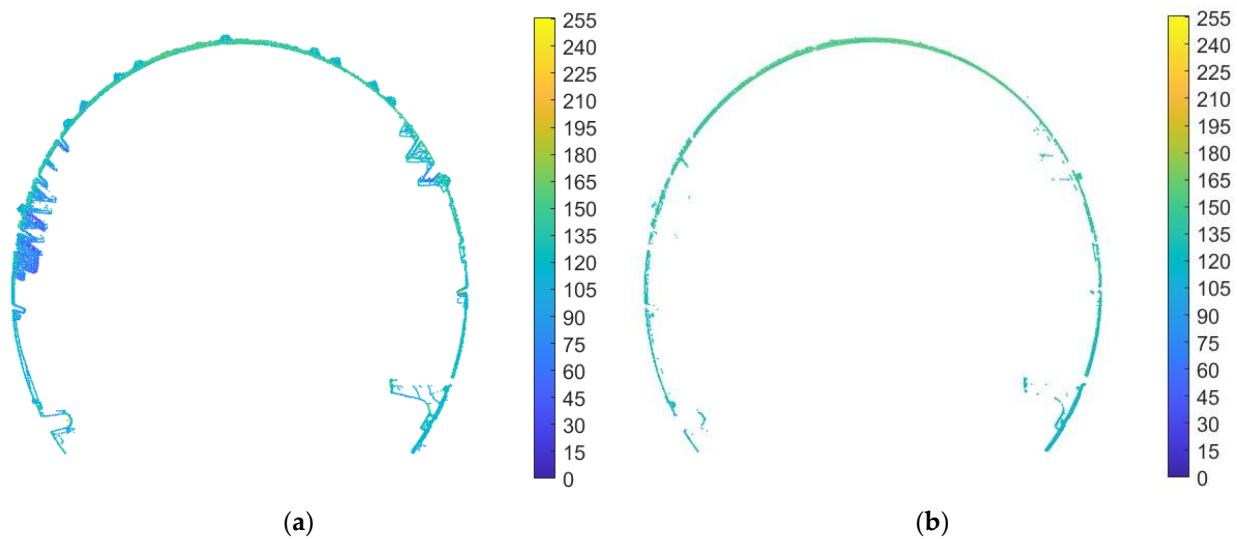


Figure 17. (a) Point cloud reflection intensity profile before denoising. (b) Point cloud reflection intensity profile after denoising.

The reflection intensity map of the point cloud after denoising is shown in Figure 18a, and the reflection intensity map of the noisy point cloud is shown in Figure 18b. The unfolded point cloud after denoising is shown in Figure 19a. We expanded the noisy point cloud, as shown in Figure 19b. It can be clearly seen from Figures 18 and 19 that the denoising algorithm achieved the almost complete removal of noise in pipelines, brackets, screw holes, and pipe assembly areas.

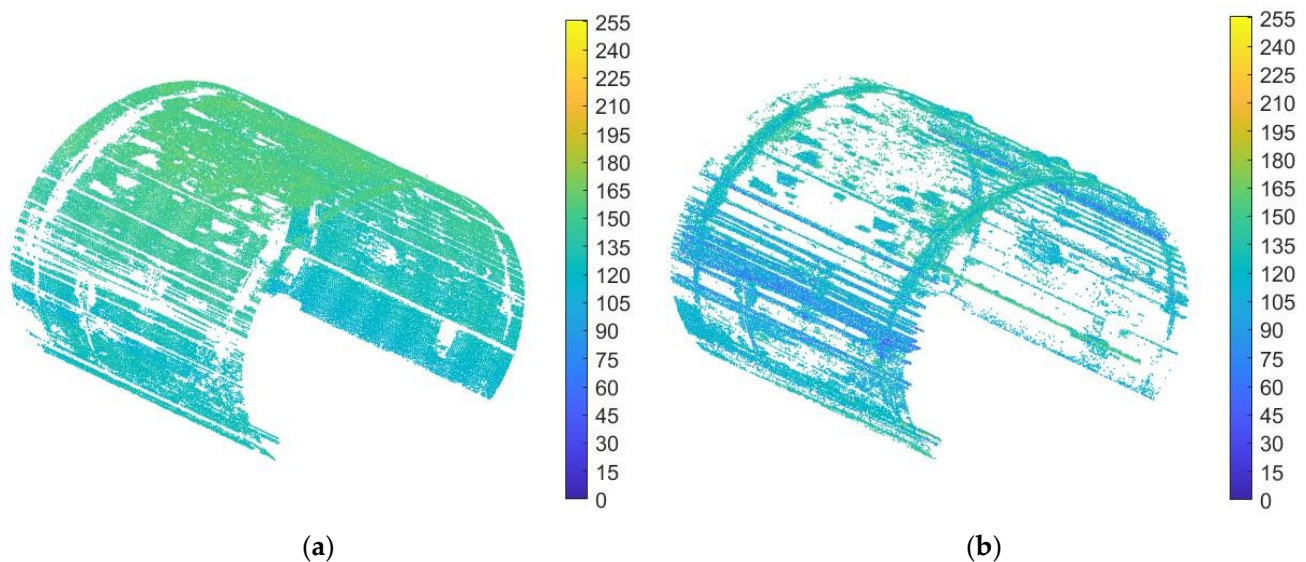


Figure 18. (a) Point cloud reflection intensity plot after denoising. (b) Noise point cloud reflection intensity plot.

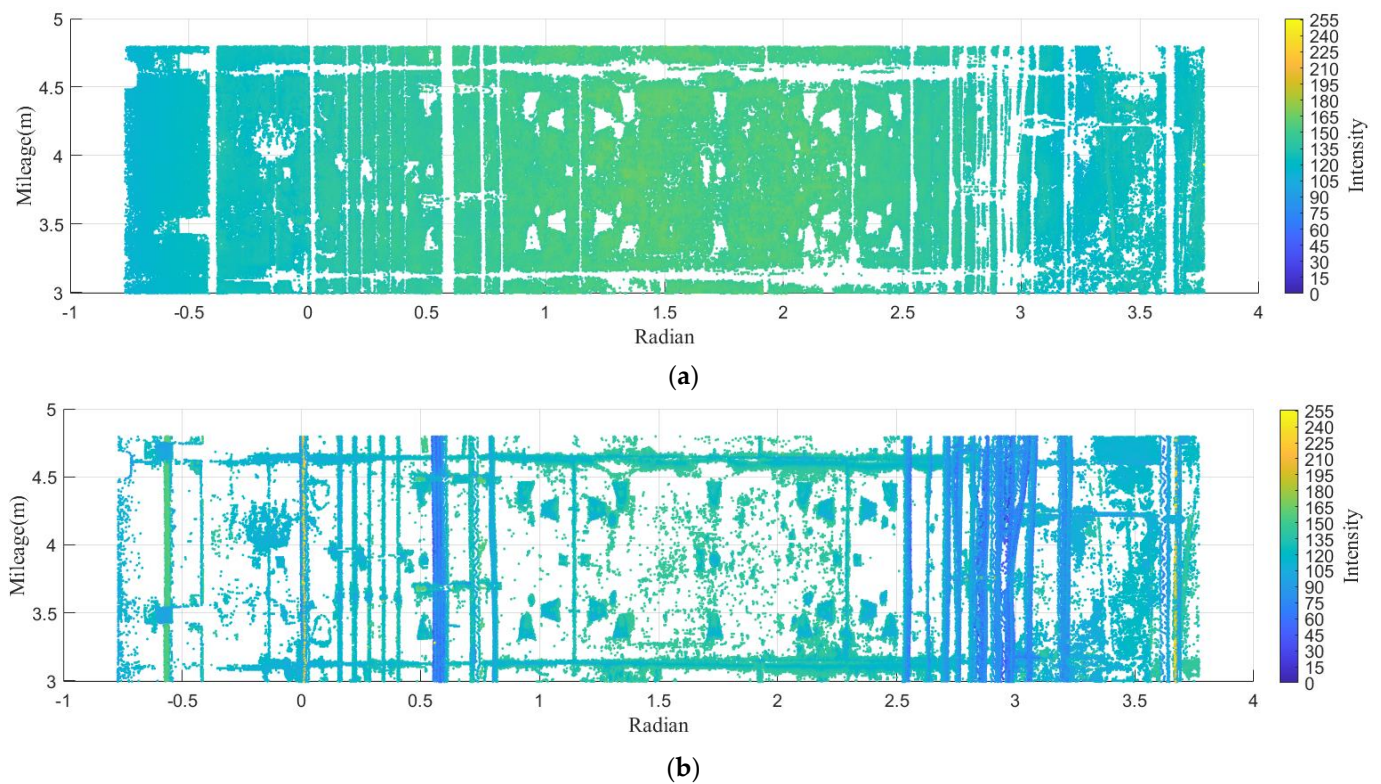


Figure 19. (a) Point cloud unfolded diagram after denoising. (b) Unfolded diagram of the tunnel noise point cloud.

The distribution map of the point cloud intensity after denoising is shown in Figure 20a. The point cloud intensity distribution of noise is shown in Figure 20b. From Figure 20b, it can be seen that the point cloud within the intensity threshold contained a large amount of noise, which could not be denoised solely by relying on the intensity threshold.

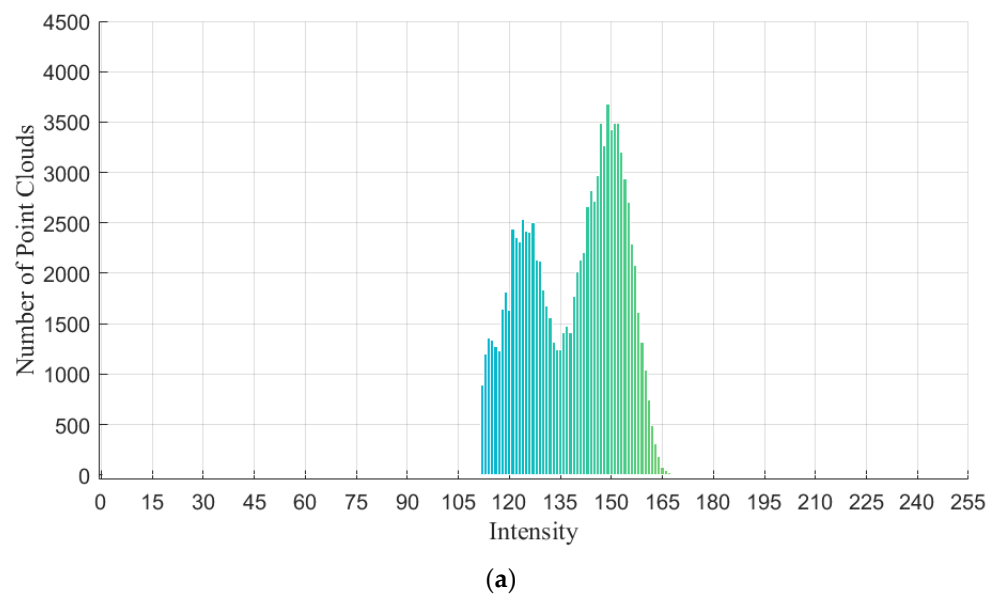


Figure 20. Cont.

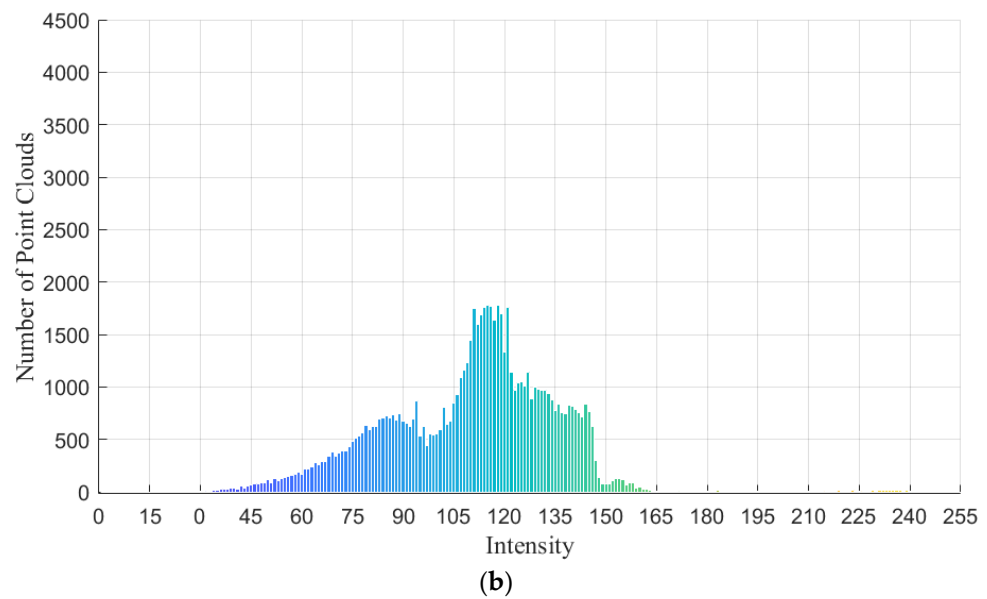


Figure 20. (a) Point cloud intensity distribution after denoising. (b) Point cloud intensity distribution of noise points (the color is rendered as intensity value, and the chromatogram is as shown in Figure 8a).

According to the method in Section 2.5, we applied geometric shape denoising to the point cloud. First, we performed elliptical fitting on the denoised segment point cloud data to obtain the center position of the segment [24,25]. We increased or decreased the design radius of the shield tunnel segment by a certain value at the center point of the segment, forming a circular range of inner and outer circle. We considered the points outside the ring as noise, while retaining the points inside the ring, as shown in Figure 21.

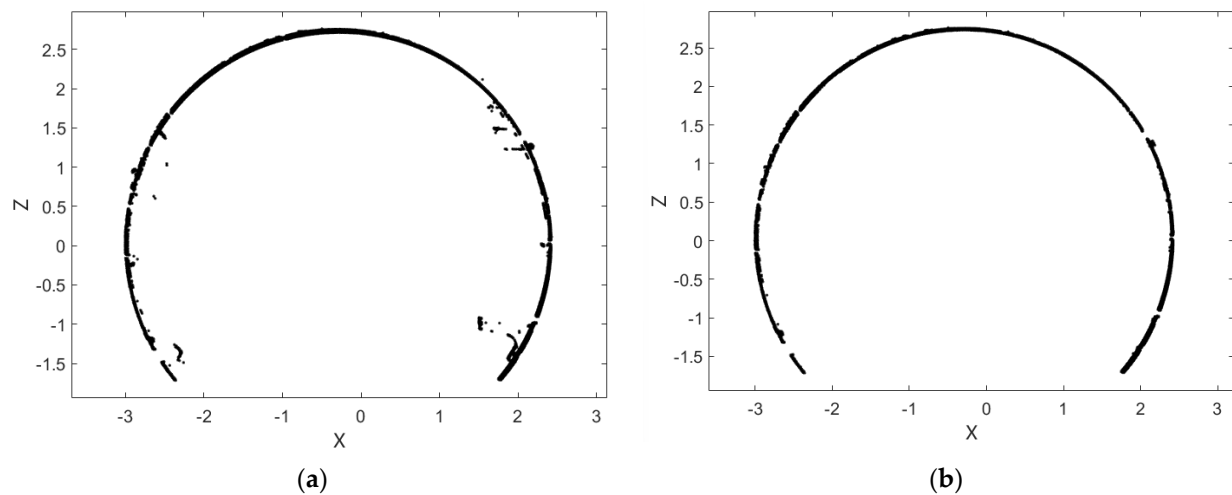


Figure 21. (a) Point cloud before design radius threshold denoising. (b) Point cloud after design radius threshold denoising.

After denoising, when zooming in on the point cloud data, protrusions and unevenness could still be observed, as shown in Figure 22. This was because in the denoising processing, a threshold based on the tunnel design radius was used. However, due to the deformation of the segments, some noise that should have been removed may still have remained in the data.

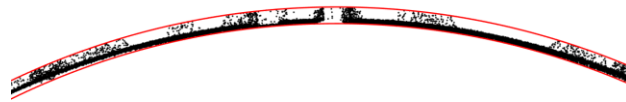


Figure 22. Point cloud within the threshold (red is the threshold boundary.).

Next, we fit the ellipse to the point cloud data of the tunnel segment and obtained the center point and ellipse equation of the tunnel segment. We increased and decreased the major and minor axes of the ellipse by a certain value to obtain two ellipses, one large and one small, forming a circular range. We considered the points outside the ring as noise, while retaining the points inside the ring, as shown in Figure 23. After denoising, we zoomed in on the details of the point cloud, as shown in Figure 24. From the figure, it can be seen that there were no protrusions or other noise points in the segment point cloud data.

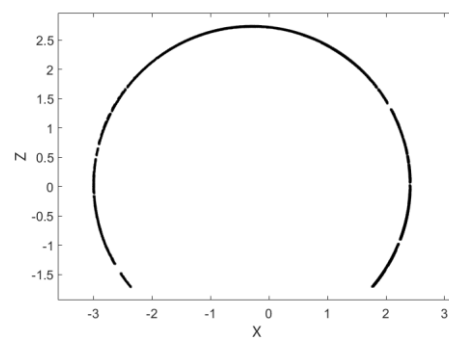


Figure 23. After elliptic threshold denoising.

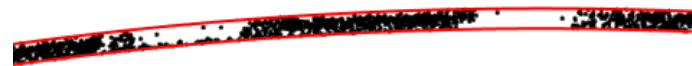


Figure 24. Point cloud within ellipse threshold (red is the threshold boundary.).

4. Discussion

In order to verify the reliability of the denoising method in the paper, this section will verify it in three ways. First, the most intuitive method was to visualize the point cloud and observe the visual effect of the point cloud data before and after denoising, as shown in Figure 25. For example, the visual effect of denoising could be evaluated by observing the smoothness, detail retention, shape changes, and other aspects of the point cloud.

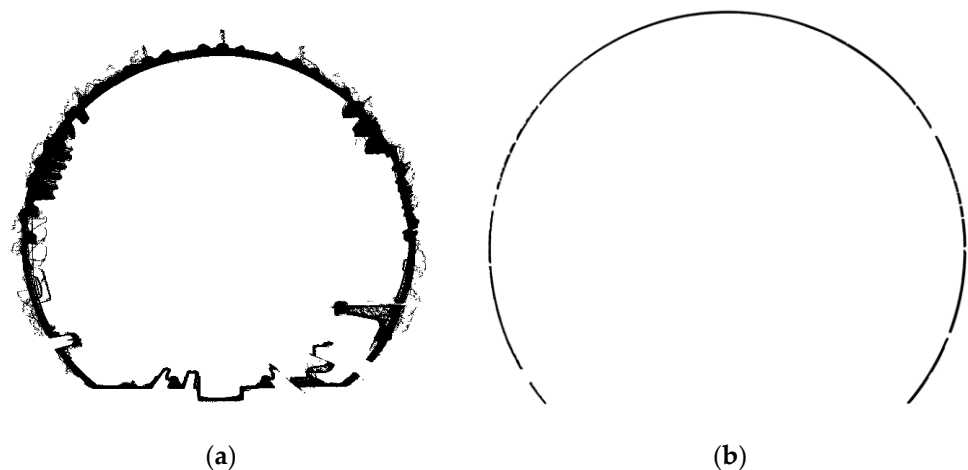


Figure 25. (a) Point cloud before denoising. (b) Point cloud after denoising.

The second method of verification was to calculate the noise removal rate for evaluation. The noise removal rate quantifies the algorithm's ability to remove noise by calculating the proportion or percentage of noise successfully removed by the denoising algorithm in the total noise. The noise removed by manual denoising is regarded as all the noise in the point cloud. Every point in the tunnel point cloud was numbered. According to the corresponding number of each point, the noise removed by this algorithm accounted for 99.77% of all noise. It was proved that the denoising effect of this algorithm was excellent. In the correspondence of each point number, it was found that the points removed by the algorithm contained some non-noise points. This paper verifies whether this will affect the denoising effect by cross-section shape preservation.

In the third method, this paper evaluates the degree to which the algorithm maintained the tunnel cross-section shape by cross-section shape preservation. This could be achieved by calculating the shape deviation between the denoised point cloud and the manually denoised point cloud. Ellipse fitting was carried out on the denoised two groups of point clouds, and the major axis and minor axis of the ellipse were obtained. The quantitative results of shape deviation were calculated by the major axis and minor axis of two fitted ellipses. The maximum relative deviation (MRD) is defined as the maximum relative difference between this method and manually denoised point cloud fitted elliptical data. The average deviation (AD) is defined as the average deviation between this method and manually denoised point cloud fitted elliptical data. The mean squared error (MSE) is defined as the mean squared error between this method and manually denoised point cloud fitted elliptical data, as shown in Equation (3). The comparison results of two fitted ellipse data are shown in Table 1. The results indicated that the shape deviation was small and the cross-section shape preservation was good. At the same time, it was proved that some non-noise points removed by the algorithm had no influence on the denoising effect.

$$\begin{aligned} MRD &= \max\left(\frac{|\hat{R} - R|}{R}\right), \\ AD &= \frac{1}{n} \sum_{i=1}^n |\hat{R}_i - R_i|, \\ MSE &= \frac{1}{n} \sum_{i=1}^n [\hat{R}_i - R_i]^2, \end{aligned} \quad (3)$$

In the equations,

\hat{R}_i represents the ellipse fitting data obtained from manual denoising,

R_i represents the ellipse fitting data obtained from filtering denoising.

Table 1. Comparison of indicators.

Comparison Parameters	MRD	AD	MSE
Major semi-axis	3.20×10^{-4}	1.47×10^{-4}	3.66×10^{-8}
Minor semi-axis	4.00×10^{-4}	3.77×10^{-4}	1.65×10^{-7}

The algorithm took 2 min to denoise the single-ring point cloud (the algorithm is operated on i5 processor by Matlab2022b), while the manual denoising took 15 min. In this paper, the experimental tunnel was 575 m long, including 383 ring segments. Theoretically, if the algorithm processed 16 single-ring point clouds in parallel, it would take 47 min to process the point cloud data of this tunnel. According to the computer performance, the algorithm could achieve higher efficiency by processing more single-ring point clouds in parallel. This paper proves the reliability of the algorithm results from three methods and verifies that the algorithm can be used as the basis for realizing efficient, comprehensive, and automatic tunnel measurement.

5. Conclusions

As crucial infrastructure for carrying a large number of passengers in their daily lives, the safe operation of subway tunnels is crucial. In order to achieve the efficient, accurate, and automated daily maintenance and testing of subway shield tunnels, at present, the mobile 3D laser scanner is used to scan the subway shield tunnel. A large amount of point cloud data is obtained by scanning, but the point cloud data contain noise. Artificial denoising is inefficient. In order to obtain high-quality point cloud data efficiently, this paper proposes a denoising method. The conclusion of this paper is as follows:

1. Based on the respective characteristics of the geometric shape and reflection intensity of the tunnel point cloud and their correlation, this paper proposes a tunnel point cloud denoising method. The method includes the following three parts: reflection intensity threshold denoising, joint shape and reflection intensity denoising, and shape denoising. The denoising process not only preserves the original surface features of the shield tunnel segments but also removes non-line-of-sight noise (caused by obstruction from pipelines, tracks, and signal equipment) and other noise (caused by bolt holes, etc.) that may affect the survey results. The experimental results showed that the method proposed in this paper achieved the same denoising effect faster than manual denoising. The denoised tunnel point cloud data can meet the requirements of daily maintenance and survey work.
2. The denoising method proposed in this paper, which combines shape and reflection intensity, plays a major role. This method takes into account the correlation between the geometric shape of the tunnel and the reflection intensity of the point cloud. By using optimized quartile range and Z-score methods to process the reflection intensity of point cloud data, noise can be effectively removed. Compared with all the noise removed by the method proposed in this paper, the combined shape and reflection intensity denoising method removed 92.1% of all the noise. This method is also applicable to other situations where the strength values vary uniformly, such as the measurement of circular shield working shaft.

The method proposed in this paper successfully removed the noise in the point cloud of shield tunnel. After verifying its practical application, it was found that it met the requirements of tunnel point cloud data surveys and could provide support for the efficient, accurate, and automated daily maintenance and survey of issues in tunnels. However, it is worth noting that the point cloud denoising method proposed in this paper mainly focuses on the point cloud denoising of straight tunnel segments. Therefore, future research will focus on point cloud denoising of curved sections of tunnels in order to realize point cloud denoising for the entire tunnel line so as to better support the daily maintenance and survey work of tunnels.

Author Contributions: Conceptualization, Y.W.; methodology, Y.W.; software, Y.W.; validation, Y.W. and D.Z.; formal analysis, Y.W.; investigation, Y.W. and L.W.; resources, C.T., Y.B., Z.S. and L.W.; data curation, Y.W.; writing—original draft preparation, Y.W.; writing—review and editing, X.M., Y.B. and Z.S.; visualization, Y.W.; supervision, X.M., Y.B., Z.S. and C.T.; project administration, Y.W. and D.Z.; funding acquisition, Y.B. All authors have read and agreed to the published version of the manuscript.

Funding: This research was funded by the National Natural Science Foundation of China, grant numbers 51829801 and 52378385.

Institutional Review Board Statement: Not applicable.

Informed Consent Statement: Not applicable.

Data Availability Statement: The data presented in this study are available on request from the corresponding author.

Acknowledgments: The first author would like to thank Liangliang Hu and Li Wang for providing some suggestions to improve the paper.

Conflicts of Interest: Author Chao Tang was employed by the company Beijing Urban Construction Exploration & Surveying Design Research Institute Co., Ltd. The remaining authors declare that the research was conducted in the absence of any commercial or financial relationships that could be construed as a potential conflict of interest.

References

1. Wu, J.; Liu, X. The Subway Construction and the Evolution of Urban Spatial Structure from the Spatial Economic Perspective. *Mod. Econ. Res.* **2023**, 85–100. [\[CrossRef\]](#)
2. Zhu, G.; Ye, M. Research on the method of point cloud denoising based on curvature characteristics and quantitative evaluation. *Bull. Surv. Mapp.* **2019**, 105–108. [\[CrossRef\]](#)
3. Zhao, F. Point cloud denoising algorithm with geometric feature preserving. *Multimed. Syst.* **2022**, 28, 1679–1687. [\[CrossRef\]](#)
4. Zaman, F.; Wong, Y.P.; Ng, B.Y. Density-Based Denoising of Point Cloud. In *9th International Conference on Robotic, Vision, Signal Processing and Power Applications: Empowering Research and Innovation*; Springer: Singapore, 2017; Volume 398, pp. 287–295.
5. Zhang, Y.; Wang, X.; Li, Q.; Yan, F. A new section line extraction method of ring forgings based on normal vector and L1-median. *Measurement* **2021**, 184, 109894. [\[CrossRef\]](#)
6. Liu, Y.; Cai, S.; Chen, Y.; Xu, Z. Point Cloud Denoising Algorithm Based on Hybrid Filtering and Improved Bilateral Filtering. *J. Northeast. Univ. (Nat. Sci.)* **2023**, 44, 682–688.
7. Wei, M.; Yu, J.; Pang, W.; Wang, J.; Qin, J.; Liu, L.; Heng, P. Bi-Normal Filtering for Mesh Denoising. *IEEE Trans. Vis. Comput. Graph.* **2015**, 21, 43–55. [\[CrossRef\]](#) [\[PubMed\]](#)
8. Mattei, E.; Castrodad, A. Point Cloud Denoising via Moving RPCA. *Comput. Graph. Forum* **2017**, 36, 123–137. [\[CrossRef\]](#)
9. Dai, S.; Dong, Q.; Ji, W.; Li, G.; Ren, Y.; Jia, R. Denoising algorithm for scattered point clouds based on normal correction and position filtering. *Transducer Microsyst. Technol.* **2023**, 42, 130–134.
10. Zheng, Y.; Li, G.; Wu, S.; Liu, Y.; Gao, Y. Guided point cloud denoising via sharp feature skeletons. *Vis. Comput.* **2017**, 33, 857–867. [\[CrossRef\]](#)
11. Liang, X.H.; Liang, J.; Guo, C. Scatter Point Cloud Denoising Based on Self-Adaptive Optimal Neighborhood. *Adv. Mater. Res.* **2010**, 97–101, 3631–3636. [\[CrossRef\]](#)
12. Gao, X.; Hu, W.; Guo, Z. Graph-based Point Cloud Denoising. In Proceedings of the 2018 IEEE Fourth International Conference on Multimedia Big Data (Bigmm), Xi'an, China, 13–16 September 2018.
13. Sun, Y.; Schaefer, S.; Wang, W. Denoising point sets via L0 minimization. *Comput. Aided Geom. Des.* **2015**, 35–36, 2–15. [\[CrossRef\]](#)
14. Li, Z.; Pan, W.; Wang, S.; Tang, X.; Hu, H. A point cloud denoising network based on manifold in an unknown noisy environment. *Infrared Phys. Technol.* **2023**, 132, 104735. [\[CrossRef\]](#)
15. Yan, J.; Zhou, L.; Wang, J.; Wang, X.; Liu, X. Structural Feature-Preserving Point Cloud Denoising Method for Aero-Engine Profile. *Int. J. Aerosp. Eng.* **2022**, 2022, 9565062. [\[CrossRef\]](#)
16. Irfan, M.A.; Magli, E. Exploiting color for graph-based 3D point cloud denoising. *J. Vis. Commun. Image Represent.* **2021**, 75, 103027. [\[CrossRef\]](#)
17. Cao, X.; Lin, Z.; Song, S.; Wang, B.; He, D.; Liu, Z. Multispectral LiDAR Point Cloud Denoising Based on Color Clustering. *Laser Optoelectron. Prog.* **2021**, 58, 483–490.
18. Choi, Y.; Jang, Y.; Lee, H.; Cho, G. Three-Dimensional LiDAR Data Classifying to Extract Road Point in Urban Area. *IEEE Geosci. Remote Sens.* **2008**, 5, 725–729. [\[CrossRef\]](#)
19. Clode, S.; Rottensteiner, F.; Kootsookos, P.; Zelniker, E. Detection and Vectorization of Roads from Lidar Data. *Photogramm. Eng. Remote Sens.* **2007**, 73, 517–535. [\[CrossRef\]](#)
20. Bao, Y.; Bom, K.I.; Li, W.; Zhang, D.; Gao, L. Detection Method for Metro Shield Tunnel Inner-ring Segment Staggering and Joint Opening Based on Point Cloud. *Urban Mass Transit* **2023**, 26, 143–149.
21. Jassim, F.A. Image Denoising Using Interquartile Range Filter with Local Averaging. *arXiv* **2013**, arXiv:1302.1007.
22. Andrade, C. Z Scores, Standard Scores, and Composite Test Scores Explained. *Indian J. Psychol. Med.* **2021**, 43, 555–557. [\[CrossRef\]](#)
23. Zhong, L.; Gao, X.; Dancigs, E.; Chang, Y. Tunnel Section Extraction and Deformation Analysis Based on Mobile Laser Scanning. In Proceedings of the 2019 6th International Conference on Systems and Informatics (ICSAI), Shanghai, China, 2–4 November 2019; pp. 1515–1521.
24. Fitzgibbon, A.; Pilu, M.; Fisher, R.B. Direct least square fitting of ellipses. *IEEE Trans. Pattern Anal.* **1999**, 21, 476–480. [\[CrossRef\]](#)
25. WalterGander; Golub, G. RolfStrebel Least-squares fitting of circles and ellipses. *Bit* **1994**, 34, 558–578.

Disclaimer/Publisher's Note: The statements, opinions and data contained in all publications are solely those of the individual author(s) and contributor(s) and not of MDPI and/or the editor(s). MDPI and/or the editor(s) disclaim responsibility for any injury to people or property resulting from any ideas, methods, instructions or products referred to in the content.